Hung RJ, McKay JD, Gaborieau V, Boffetta P, Hashibe M, Zaridze D, Mukeria A, Szeszenia-Dabrowska N, Lissowska J, Rudnai P, Fabianova E, Mates D, Bencko V, Foretova L, Janout V, Chen C, Goodman G, Field JK, Liloglou T, Xinarianos G, Cassidy A, McLaughlin J, Liu G, Narod S, Krokan HE, Skorpen F, Elvestad MB, Hveem K, Vatten L, Linseisen J, Clavel-Chapelon F, Vineism P, Bueno-de-Mesquita HB, Lund E, Martinez C, Bingham S, Rasmuson T, Hainaut P, Riboli E, Ahrens W, Benhamou S, Lagiou P, Trichopoulos D, Holcátová I, Merletti F, Kjaerheim K, Agudo A, Macfarlane G, Talamini R, Simonato L, Lowry R, Conway DI, Znaor A, Healy C, Zelenika D, Boland A, Delepine M, Foglio M, Lechner D, Matsuda F, Blanche H, Gut I, Heath S, Lathrop M, Brennan P.	A susceptibility locus for lung cancer maps to nicotinic acetylcholine receptor subunit genes on 15q25.	**Nature**.	452,	633-637	2008
Gotoh N, Yamada R, Matsuda F, Yoshimura N, Iida, T.	Manganase superoxide dismutase gene (SOD2) polymorphism and exudative age-related macular degeneration in the Japanese population.	**Am. J. Ophthalmol**.	146	146-147	2008

Trégouet DA, Groop PH, McGinn S, Forsblom C, Hadjadj S, Marre M, Parving HH, Tarnow L, Telgmann R, Godefroy T, Nicaud V, Rousseau R, Parkkonen M, Hoverfält A, Gut I, Heath S, Matsuda F, Cox R, Kazeem G, Farrall M, Gauguier D, Brand-Herrmann SM, Cambien F, Lathrop M, Vionnet N. For the EURAGEDIC Consortium.	G/T substitution in intron-1 of UNC13B gene is associated with increased risk of nephropathy in patients with type 1 diabetes.	**Diabetes.**	57(10)	2843-50	2008
The SEARCH Collaborative Group, Link E, Parish S, Armitage J, Bowman L, Heath S, Matsuda F, Gut I, Lathrop M, Collins R.	SLCO1B1 variants and statin-induced myopathy--a genomewide study.	**N. Engl. J. Med.**	359	789-799	2008
Yamano E, Isowa T, Nakano Y, Matsuda F, Hashimoto-Tamaoki T, Ohira H, Kosugi S.	Association study between reward dependence temperament and a polymorphism in the phenylethanolamine N-methyltransferase gene in a Japanese female population.	**Compr. Psychiatry.**	49	503-507	2008
Poupon R, Ping C, Chrétien Y, Corpechot C, Chazouillères O, Simon T, Heath SC, Matsuda F, Poupon RE, Housset C, Barbu V.	Genetic factors of susceptibility and of severity in primary biliary cirrhosis.	**J. Hepatol.**	49(6)	1038-45	2008
Gotoh N, Yamada R, Nakanishi H, Saito M, Iida T, Matsuda F, Yoshimura N.	Correlation between CFH Y402H and HTRA1 rs11200638 genotype to typical exudative age-related macular degeneration and polypoidal choroidal vasculopathy phenotype in the Japanese population.	**Clin. Experiment. Ophthalmol.**	36	437-42	2008

McKay JD, Hung RJ, Gaborieau V, Boffetta P, Chabrier A, Byrnes G, Zaridze D, Mukeria A, Szeszenia-Dabrowska N, Lissowska J, Rudnai P, Fabianov E, Mates D, Bencko V, Foretova L, Janout V, McLaughlin J, Shepherd F, Montpetit A, Narod S, Krokan HE, Skorpen F, Elvestad MB, Vatten L, Njølstad I, Axelsson T, Chen C, Goodman G, Barnett M, Loomis MM, Lubiński J, Matyjasik J, Lener M, Oszutowska D, Field J, Liloglou T, Xinarianos G, Cassidy A; EPIC Study, Vineis P, Clavel-Chapelon F, Palli D, Tumino R, Krogh V, Panico S, González CA, Ramón Quirós J, Martínez C, Navarro C, Ardanaz E, Larrañaga N, Kham KT, Key T, Bueno-de-Mesquita HB, Peeters PH, Trichopoulou A, Linseisen J, Boeing H, Hallmans G, Overvad K, Tjønneland A, Kumle M, Riboli E, Zelenika D, Boland A, Delepine M, Foglio M, Lechner D, Matsuda F, Blanche H, Gut I, Heath S, Lathrop M, Brennan P.	Lung cancer susceptibility locus at 5p15.33.	**Nat Genet.**	40(12)	1404-6	2008
Taniguchi T, Hamasaki A, Okamoto M.	Subclinical hypercortisolism in hospitalized patients with type 2 diabetes mellitus.	**Endocr J.**	55	429-32	2008

Koshiyama H, Taniguchi A, Tanaka K, Kagimoto S, Fujioka Y, Hirata K, Nakamura Y, Iwakura A, Hara K, Yamamoto T, Kuroe A, Ohya M, Fujimoto S, Hamamoto Y, Honjo S, Ikeda H, Nabe K, Tsuda K, Inagaki N, Seino Y, Kume N.	Effect of pitavastatin on lipid profile and high-sensitivy CRP in Japanese subjects with hypercholesterolemia: Kansai Investigation of Statin for Hyperlipidemic Intervention in Metabolism and Endocrinology (KISHIMEN) Investigators.	**J Atheroscler Thromb.**	15	345-350	2008
Gu N, Tsuda M, Matsunaga T, Adachi T, Yasuda K, Ishihara A, Tsuda K.	Glucose regulation of dipeptidyl peptidase IV gene expression is mediated by hepatocyte nuclear factor-1alpha in epithelial intestinal cells.	**Clin Exp Pharmacol Physiol.**	35(12)	1433-9	2008

DIABETES RESEARCH AND CLINICAL PRACTICE 82 (2008) 353–358

available at www.sciencedirect.com

ScienceDirect

journal homepage: www.elsevier.com/locate/diabres

Analysis of factors influencing pancreatic β-cell function in Japanese patients with type 2 diabetes: Association with body mass index and duration of diabetic exposure

Shogo Funakoshi[a], *Shimpei Fujimoto*[a,*], *Akihiro Hamasaki*[a], *Hideya Fujiwara*[a], *Yoshihito Fujita*[a], *Kaori Ikeda*[a], *Yoshiyuki Hamamoto*[a], *Masaya Hosokawa*[a], *Yutaka Seino*[b], *Nobuya Inagaki*[a]

[a] *Department of Diabetes and Clinical Nutrition, Graduate School of Medicine, Kyoto University, 54 Shogoin Kawahara-cho, Sakyo-ku, Kyoto 606-8507, Japan*

[b] *Kansai Electric Power Hospital, Osaka, Japan*

ARTICLE INFO

Article history:
Received 19 March 2008
Received in revised form
25 August 2008
Accepted 8 September 2008
Published on line 23 October 2008

Keywords:
Type 2 diabetes
C-peptide
β-Cell
BMI
Disease duration

ABSTRACT

Aims: To elucidate the clinical factors affecting β-cell function, serum C-peptide immunoreactivity (CPR) levels of patients with type 2 diabetes were analyzed.

Methods: Seven hundred Japanese patients with type 2 diabetes were enrolled. β-Cell function was evaluated by fasting CPR (FCPR), 6 min after intravenous injection of 1 mg glucagon (CPR-6 min), and the increment of CPR (ΔCPR). Simple regression analysis between FCPR, CPR-6 min, and ΔCPR and measures of variables and stepwise multiple regression analysis were carried out.

Results: Years from diagnosis and BMI were the major independent variables predicting β-cell function. Years from diagnosis was negatively correlated with CPR-6 min ($P < 0.0001$, $r = -0.271$), and decrease in CPR-6 min was 0.050 ng/(ml year). BMI was positively correlated with CPR-6 min ($P < 0.0001$, $r = 0.369$). When subjects were divided according to BMI, the decrease in CPR-6 min per year in the high-BMI group (0.068 ng/(ml year)) was greater than that in the low-BMI group (0.035 ng/(ml year)).

Conclusion: A linear decline in endogenous insulin secretion over more than several decades of diabetes was confirmed by this cross-sectional study. The duration of diabetes exposure and BMI are thus major factors in β-cell function in Japanese patients with type 2 diabetes.

1. Introduction

Type 2 diabetes is a heterogeneous disease characterized by insulin resistance and defective insulin secretion [1], and is progressive in that therapy must be altered over time. Initially upon diagnosis, diet and exercise are generally adequate to achieve glycemic control. Oral hypoglycemic agents (OHA) are later required when patients cannot achieve glycemic control with diet and exercise. Daily insulin injection is finally indicated when patients are unable to achieve glycemic control with a combination of oral agents, diet, and exercise [2,3]. These requirements may well be, at least in part, due to progressive loss of pancreatic β-cell function. The results of the United Kingdom Prospective Diabetes Study (UKPDS) shows that pancreatic β-cell function (%β), assessed by Homeostasis Model Assessment (HOMA) in patients allocated

* *Corresponding author.* Tel.: +81 75 751 3560; fax: +81 75 751 4244.
E-mail address: fujimoto@metab.kuhp.kyoto-u.ac.jp (S. Fujimoto).

0168-8227/$ – see front matter
doi:10.1016/j.diabres.2008.09.010

to diet or OHA, decreased approximately 25% in 5 years [4]. However, the effect of more prolonged duration of diabetic exposure on β-cell function including the insulin-requiring stage has not been determined. It has been proposed that the β-cell secrets additional insulin to compensate for increasing insulin resistance to maintain normal glucose tolerance [5]. However, the effect of insulin resistance on β-cell function in diabetes remains largely unknown.

In the present study, to evaluate the clinical factors affecting β-cell function by cross-sectional study, serum C-peptide immunoreactivity levels of patients with type 2 diabetes including insulin-requiring patients were analyzed.

2. Subjects and methods

2.1. Study subjects

Seven hundred ninety-eight Japanese patients with type 2 diabetes admitted between 1997 and 2007 to Kyoto University Hospital for poor glycemic control were enrolled in the study. Type 2 diabetes mellitus was diagnosed based on the criteria of the American Diabetes Association [6]. Patients with pancreatic disease, liver disease, or those taking diabetogenic medication were excluded. Patients with serum creatinine ≥1.3 mg/dl were excluded, as serum C-peptide immunoreactivity (CPR) is elevated by decreased renal function [7]. Seven hundred patients were enrolled. Age and BMI (mean ± S.E.) were 62.2 ± 0.5 years and 24.1 ± 0.1 kg/m^2, respectively. Years from diagnosis was 11.1 ± 0.4; HbA_{1C} at admission was 9.3 ± 0.1%. Systolic and diastolic blood pressure were 122.6 ± 0.5 and 73.3 ± 0.4 mmHg, respectively. The number of patients treated with diet alone, oral hypoglycemic agents (OHA), insulin, and insulin plus OHA was 71, 225, 274, and 130, respectively.

2.2. Methods

On the first or second day in hospital, medical history, physical examination, and laboratory evaluation including glycosylated hemoglobin were performed. β-Cell function was examined within 1 week. β-Cell function was evaluated after overnight fast by glucagon test measuring CPR before [fasting CPR (FCPR)] and 6 min after intravenous injection of 1 mg glucagon (CPR-6 min) [8], as the test is valid in patients taking insulin therapy. Increment of CPR (ΔCPR) was obtained by subtracting FCPR from CPR-6 min. Serum CPR was measured by radioimmunoassay (RIA) (samples of 299 patients from 1997 to 2002 using Daiichi III, Daiichi Radioisotope Laboratories, Japan); by immunoenzymometric assay (EIA) (samples of 401 patients from 2003 to 2007 using ST AIA-PACK C-Peptide, Toso corporation, Japan). The same samples were measured by two kits, and a formula to convert the value (EIA value = 0.98 × RIA value + 0.41, $n = 161$, $r = 0.99$) was obtained. In patients taking OHA, medication was stopped for the glucagon test, but was maintained until 1 day before to prevent hyperglycemia during the test. Fasting plasma glucose was measured by glucose oxidase method when the glucagon test was performed. The date of diagnosis for patients was determined from their medical record, medical history, and previous clinical data by the criteria for the diagnosis of diabetes proposed by the American Diabetes Association [6].

2.3. Statistical analysis

Statistical analysis was performed with the StatView 5.0 system (SAS institute Inc., Cary, NC). Data are presented as mean ± S.E. The relationship between the parametric clinical data and CPR values was investigated by Pearson analysis. The relationship between the nonparametric clinical data and CPR values was investigated by Spearman analysis. Stepwise multiple regression analysis was performed. Clinical parameters among the three groups above were compared by analysis of variance (ANOVA). For comparison of two groups, Scheffe's test was performed as post hoc analysis. P values <0.05 were considered statistically significant.

3. Results

Simple correlation coefficients between FCPR, CPR-6 min, and ΔCPR and measures of variables (age, years from diagnosis, BMI, HbA_{1C}, systolic and diastolic blood pressure, serum creatinine, sex, and fasting plasma glucose) were calculated and are indicated in Table 1. Stepwise multiple regression analysis was carried out using independent variables in Table 1 to predict indexes of endogenous insulin secretion as a dependent variable (Table 2). Stepwise multiple regression analysis is indicated in Table 2. FCPR was independently predicted by years from diagnosis, BMI, and serum creatinine,

Table 1 – P value of simple correlation between indexes of endogenous insulin secretion and measures of variables.

	FCPR (ng/ml)	CPR-6 min (ng/ml)	ΔCPR (ng/ml)
Age (year)	0.0326	<0.0001	<0.0001
Years from diagnosis	<0.0001	<0.0001	<0.0001
BMI (kg/m^2)	<0.0001	<0.0001	<0.0001
Systolic blood pressure (mmHg)	0.9481	0.2091	0.0593
Diastolic blood pressure (mmHg)	0.1139	0.0044	0.0016
FPG (mg/dl)	0.0783	0.0010	0.0002
HbA_{1C} (%)	0.0375	0.2152	0.7699
sCre (mg/dl)	<0.0001	0.0836	0.3917
Sex	0.8978	0.7958	0.8206

FPG: fasting plasma glucose; sCre: serum creatinine.

Table 2 – Stepwise multiple regression analysis for predictors of indexes of endogenous insulin secretion.

	F value	Partial regression coefficient	Standard partial regression coefficient	R^2 (|R|)
FCPR (ng/ml)				
Years from diagnosis	41.4	−0.020	−0.219	0.217 (0.469)
BMI (kg/m^2)	114.4	0.087	0.362	
sCre (mg/dl)	27.7	0.877	0.179	
CPR-6 min (ng/ml)				
Years from diagnosis	45.8	−0.043	−0.233	0.198 (0.449)
BMI (kg/m^2)	102.8	0.167	0.348	
FPG (mg/dl)	10.8	0.004	0.113	
ΔCPR (ng/ml)				
Years from diagnosis	34.7	−0.025	−0.212	0.129 (0.365)
BMI (kg/m^2)	47.9	0.077	0.248	
FPG (mg/dl)	13.2	0.003	0.130	

FPG: fasting plasma glucose; sCre: serum creatinine.

accounting for 21.7% of the variability of FCPR. CPR-6 min and ΔCPR were independently predicted by years from diagnosis, BMI, and fasting plasma glucose (FPG), accounting for 19.8% and 12.9% of the variability of the dependent variables, respectively.

Scattered plots of linear regression, simple regression coefficient, and formula between indexes of endogenous insulin secretion and years from diagnosis, BMI, FPG, and serum creatinine are shown in Figs. 1–4, respectively.

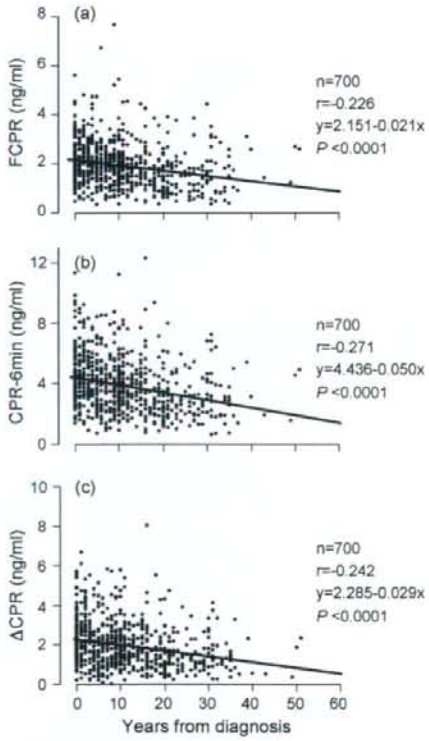

Fig. 1 – The relationship between years from diagnosis and FCPR (a), CPR-6 min (b), and ΔCPR (c).

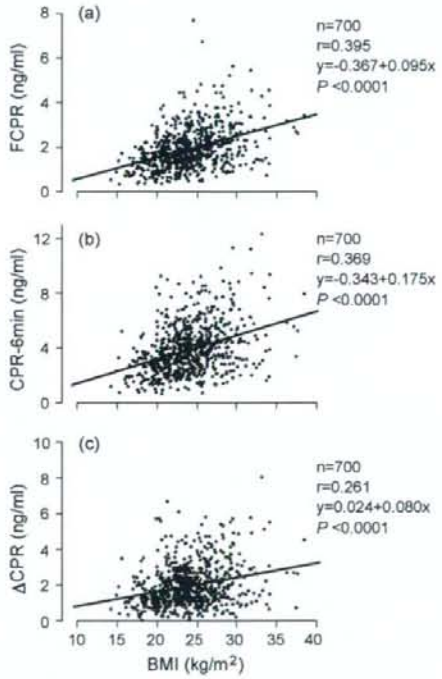

Fig. 2 – The relationship between BMI and FCPR (a), CPR-6 min (b), and ΔCPR (c).

Years from diagnosis was negatively correlated with FCPR ($P < 0.0001$, $r = -0.226$), CPR-6 min ($P < 0.0001$, $r = -0.271$), and ΔCPR ($P < 0.0001$, $r = -0.242$) (Fig. 1). The decrease in FCCP, CPR-6 min, and ΔCPR was 0.021, 0.050, and 0.029 ng/(ml year), respectively (Fig. 1). BMI was positively correlated with FCPR ($P < 0.0001$, $r = 0.395$), CPR-6 min ($P < 0.0001$, $r = 0.369$), and ΔCPR ($P < 0.0001$, $r = 0.261$) (Fig. 2). FPG was weakly correlated with CPR-6 min ($P = 0.001$, $r = 0.125$) and ΔCPR ($P = 0.0002$, $r = 0.141$) (Fig. 3). Serum creatinine was weakly correlated with FCPR ($P < 0.0001$, $r = 0.171$) (Fig. 4).

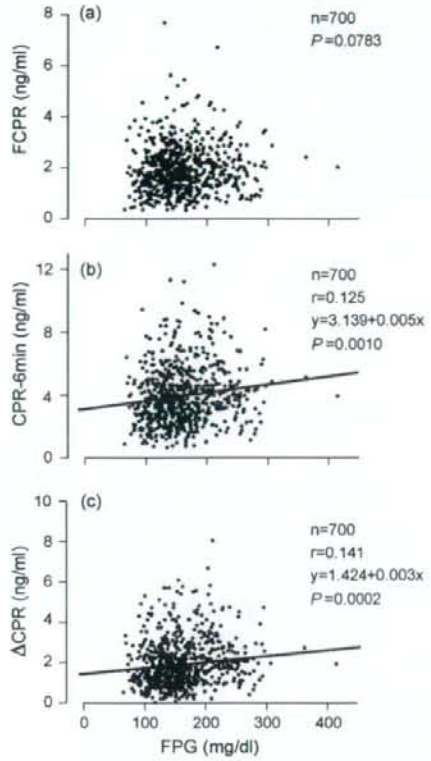

Fig. 3 – The relationship between fasting plasma glucose (FPG) and FCPR (a), CPR-6 min (b), and ΔCPR (c).

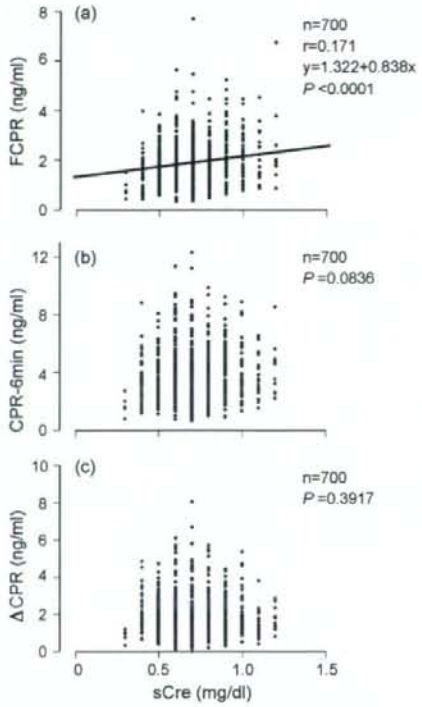

Fig. 4 – The relationship between serum creatinine (sCre) and FCPR (a), CPR-6 min (b), and ΔCPR (c).

Because BMI is the other major independent variable associated with indexes of endogenous insulin secretion, we compared the subjects divided at BMI 25.0. Single regression analysis between CPR-6 min and years from diagnosis was performed on each group. Years from diagnosis was negatively correlated with CPR-6 min in both groups (BMI < 25: $n = 430$, $P < 0.0001$, $r = -0.233$, $y = 3.876 - 0.035x$; BMI ≥ 25.0: $n = 270$, $P < 0.0001$, $r = -0.309$, $y = 5.229 - 0.067x$). The decrease in CPR-6 min per year in the high-BMI (27.9 ± 0.2 kg/m^2) group (0.067 ng/(ml year)) was greater than that in the low-BMI (21.8 ± 0.1 kg/m^2) group (0.035 ng/(ml year)). Comparison of the clinical data among four groups of increasing years from

Table 3 – Comparison of clinical characteristics and clinical profile among groups according to years from diagnosis.

Groups (years from diagnosis)	I (–9.9)	II (10.0–19.9)	III (20.0–29.9)	IV (30–)	P
Years from diagnosis	3.6 ± 0.2	13.3 ± 0.2[a]	23.4 ± 0.3[a,b]	34.0 ± 0.7[a,b,c]	<0.0001
Number of subjects	355	204	94	47	
Sex (M/F)	215/140	114/90	50/44	31/16	
Age (year)	58.4 ± 0.7	63.7 ± 0.8[a]	68.8 ± 0.9[a,b]	70.9 ± 1.2[a,b]	<0.0001
BMI (kg/m^2)	24.4 ± 0.2	24.0 ± 0.3	23.3 ± 0.3	23.9 ± 0.5	0.0912
HbA_{1c} (%)	9.5 ± 0.1	9.1 ± 0.1	9.4 ± 0.2	8.9 ± 0.2	0.0823
SBP (mmHg)	122.0 ± 0.7	122.1 ± 0.9	124.8 ± 1.5	124.8 ± 2.1	0.2163
DBP (mmHg)	75.3 ± 0.5	72.0 ± 0.6[a]	69.9 ± 0.9[a]	70.8 ± 1.3[a]	<0.0001
sCre (mg/dl)	0.70 ± 0.01	0.72 ± 0.01	0.73 ± 0.02	0.76 ± 0.03	0.0650
FPG (mg/dl)	162.9 ± 2.6	159.7 ± 3.4	154.6 ± 4.9	156.1 ± 7.5	0.4498
FCPR (ng/ml)	2.12 ± 0.05	1.83 ± 0.06[a]	1.46 ± 0.08[a,b]	1.73 ± 0.14[a]	<0.0001
CPR-6 min (ng/ml)	4.30 ± 0.10	3.75 ± 0.12[a]	2.87 ± 0.14[a,b]	3.29 ± 0.24[a]	<0.0001
ΔCPR (ng/ml)	2.18 ± 0.07	1.93 ± 0.08	1.42 ± 0.09[a,b]	1.56 ± 0.15[a]	<0.0001

FPG: fasting plasma glucose; sCre: serum creatinine; SBP: systolic blood pressure; DBP: diastolic blood pressure.
[a] $P < 0.05$ vs. group I.
[b] $P < 0.05$ vs. group II.
[c] $P < 0.05$ vs. group III.

Table 4 – Comparison of indexes of endogenous insulin secretion between low-BMI and high-BMI subjects according to years from diagnosis.

Group (year)	I (–9.9)		II (10.0–19.9)		III (20.0–29.9)		IV (30.0–)	
BMI	<25	≥25	<25	≥25	<25	≥25	<25	≥25
Number of subjects	202	153	130	74	66	28	32	15
FCPR (ng/ml)	1.82 ± 0.06	2.52 ± 0.07*	1.66 ± 0.06	2.12 ± 0.12*	1.35 ± 0.09	1.72 ± 0.14	1.67 ± 0.15	1.85 ± 0.27
CPR-6 min (ng/ml)	3.83 ± 0.12	4.99 ± 0.15*	3.41 ± 0.12	4.33 ± 0.25*	2.70 ± 0.16	3.15 ± 0.26	3.20 ± 0.27	3.48 ± 0.50
ΔCPR (ng/ml)	2.00 ± 0.09	2.46 ± 0.11*	1.76 ± 0.08	2.21 ± 0.16*	1.38 ± 0.10	1.50 ± 0.17	1.54 ± 0.18	1.63 ± 0.27

P values were analyzed by unpaired Student *t* test.
* $P < 0.01$ vs. low-BMI patients.

diagnosis (–9.9 years, 10.0–19.9 years, 20.0–29.9 years, and 30.0– years) is shown in Table 3. Age, diastolic blood pressure, FCPR, CPR-6 min, and ΔCPR were significantly different among the groups. Comparison between the high-BMI and low-BMI subjects in the four groups of increasing years from diagnosis shows that FCPR, CPR-6 min, and ΔCPR were significantly increased in high-BMI subjects with years from diagnosis less than 19.9, while this was not the case when years from diagnosis was more than 20.0 (Table 4).

4. Discussion

While the present study should be interpreted carefully since it is a cross-sectional rather than a longitudinal study, we have shown that endogenous insulin secretory capacity in Japanese patients with type 2 diabetes is more closely associated with variables including years from diagnosis which reflects longer term diabetes exposure, than with variables including HbA_{1c} that reflect shorter term diabetes exposure. A decline of indexes of endogenous insulin secretion during more than several decades of diabetes was confirmed in this cross-sectional study, as was found in the longitudinal 5-year UKPDS study, although the decline became gradual. BMI is also an important independent variable to predict CPR level in type 2 diabetes.

The key role of pancreatic β-cell function in the pathogenesis of type 2 diabetes is increasingly apparent. Weyer et al. has established that impaired insulin secretion is associated with conversion from normal glucose tolerance (NGT) to impaired glucose tolerance (IGT) in a longitudinal study of Pima Indians [5]. In other studies, it has been reported that insulin secretory defect is the predominant abnormality even at an early stage of decreasing glucose tolerance [9–13]. The UKPDS findings show that pancreatic β-cell function (%β), assessed by HOMA in patients with type 2 diabetes, decreased approximately 25% in 5 years [4]. Thus, pancreatic β-cell function may continue to deteriorate as glucose intolerance progresses from NGT via IGT and non-insulin-requiring diabetes progresses to insulin-requiring diabetes [14–16].

Progressive loss of pancreatic β-cell function in patients with type 2 diabetes may be derived, at least in part, from reduced pancreatic β-cell mass, which has been found in examination of pancreatic tissue at autopsy [17–19]. One study suggests that increased apoptosis is more important in reduced β-cell mass than impaired neogenesis and proliferation in type 2 diabetes [17]. Factors in deteriorating pancreatic β-cell function during diabetic exposure including hyperglycemia, hyperlipidemia, cytokines secreted by adipocytes, immune response, and medication have been proposed based mainly on *in vitro* studies [20–22], but clinical evidence of the influence of these factors on β-cell deterioration remains to be elucidated. Assessment of insulin secretory function by HOMA in UKPDS indicated that the rates of loss of insulin secretory function were similar among groups of diet-treated, sulfonylurea-treated, and metformin-treated patients [4], which may imply that progressive β-cell deterioration occurs independent of the mode of therapy. Oxidative stress in islets of patients with type 2 diabetes, which is related to hyperglycemia and causes tissue damage, is found to be increased at autopsy [18], but clinical evidence of long-term concentration-dependent effects of hyperglycemia on β-cell deterioration is lacking.

β-Cell function increases to compensate for increased insulin resistance in subjects yet maintaining normal glucose tolerance [5]. The increase in β-cell function is brought about, at least in part, by expansion of β-cell mass, which is derived from promotion of proliferation and neogenesis and from prevention of apoptosis mediated by increased activity of growth factor signaling pathways, glucose metabolism, GLP-1 signaling, and free fatty acid metabolism and signaling [22]. Since BMI is also correlated with insulin resistance estimated by homeostasis model assessment (HOMA-IR) in Japanese patients with type 2 diabetes [23], the relationship between BMI and β-cell function is of special concern. In autopsy of subjects with normal glucose tolerance, β-cell mass is found to be greater in obese than in lean subjects [17]. These findings suggest that increased BMI may be associated with increased β-cell mass and function in subjects maintaining normal glucose tolerance. The present study also suggests that BMI is positively associated with β-cell function in patients with type 2 diabetes. This result is compatible with autopsy findings of good correlation of β-cell mass with BMI [19]. Interestingly, the time-dependent decline of CPR level was steeper in obese than in lean subjects in the present study, which is compatible with the autopsy finding that the difference in β-cell volume between non-diabetic and type 2 diabetes subjects is greater in obese than in lean subjects [17]. While a decline of β-cell function of about 5% (HOMA-β%)/year was observed in subjects with average BMI of about 30 in UKPDS, the figure might well be lower in Japanese patients whose average BMI is under 25. However, direct comparison of our measure of β-cell function using CPR in a cross-sectional study with β-cell function assessed by HOMA-β in a longitudinal UKPDS study is problematic. In the present study, larger values of endogenous insulin secretion in high-BMI subjects compared with low-BMI

subjects were observed in groups with fewer years from diagnosis, suggesting that the influence of BMI on β-cell secretory function is more prominent in disease of shorter duration. One possible explanation for this phenomenon is that the compensatory β-cell mass increase with obesity is gradually lessened by long-term diabetic exposure.

The mean of indexes of endogenous insulin secretion was higher in patients with years from diagnosis more than 30 than in patients with years from diagnosis from 20 to 29.9 (Table 3), but the difference was not significant. This result might be linked to the exclusion of patients with serum creatinine above 1.3 mg/dl, who have diabetic nephropathy with renal insufficiency most likely due to the more severe and prolonged diabetic exposure.

FCPR, but not CPR-6 min and ΔCPR, is positively correlated with serum creatinine (Fig. 4). These results indicate that in the normal range of creatinine, the serum CPR level in the fasting stable state, but not the stimulated CPR level in the dynamic state, is affected by renal function, which determines CPR clearance.

In conclusion, a linear decline in endogenous insulin secretion over more than several decades of diabetes was confirmed by this cross-sectional study. The duration of diabetes exposure and BMI are major factors in β-cell function in Japanese patients with type 2 diabetes.

Acknowledgments

This study was supported in part by Scientific Research Grants, a Grant for Leading Project for Biosimulation from the Ministry of Education, Culture, Sports, Science and Technology of Japan, and a grant from CREST of Japan Science and Technology Cooperation.

Conflict of interest

There are no conflicts of interest.

REFERENCES

[1] R.A. DeFronzo, Lilly lecture 1987. The triumvirate: beta-cell, muscle, liver. A collusion responsible for NIDDM, Diabetes 37 (1988) 667–687.
[2] H. Yki-Jarvinen, M. Kauppila, E. Kujansuu, J. Lahti, T. Marjanen, L. Niskanen, et al., Comparison of insulin regimens in patients with non-insulin-dependent diabetes mellitus, N. Engl. J. Med. 327 (1992) 1426–1433.
[3] R.C. Turner, C.A. Cull, V. Frighi, R.R. Holman, Glycemic control with diet, sulfonylurea, metformin, or insulin in patients with type 2 diabetes mellitus: progressive requirement for multiple therapies (UKPDS 49), UK Prospective Diabetes Study (UKPDS) Group, JAMA 281 (1999) 2005–2012.
[4] U.K. Prospective Diabetes Study Group, U.K. prospective diabetes study 16. Overview of 6 years' therapy of type II diabetes: a progressive disease, Diabetes 44 (1995) 1249–1258.
[5] C. Weyer, C. Bogardus, D.M. Mott, R.E. Pratley, The natural history of insulin secretory dysfunction and insulin resistance in the pathogenesis of type 2 diabetes mellitus, J. Clin. Invest. 104 (1999) 787–794.
[6] American Diabetes Association, Diagnosis and classification of diabetes mellitus, Diabetes Care 30 (Suppl. 1) (2007) S42–S47.
[7] H. Kajimuma, S. Tanabashi, K. Ishiwata, N. Kuzuya, Urinary excretion of C-peptide in relation to renal function, in: S. Baba (Ed.), Proinsulin, Insulin C-peptide, Excerpta Medica, Amsterdam, 1979, pp. 183–189.
[8] O.K. Faber, C. Binder, C-peptide response to glucagons, A test for the residual β-cell function in diabetes mellitus, Diabetes 26 (1977) 605–610.
[9] H. Yoneda, H. Ikegami, Y. Yamamoto, E. Yamato, T. Cha, Y. Kawaguchi, et al., Analysis of early-phase insulin responses in nonobese subjects with mild glucose intolerance, Diabetes Care 15 (1992) 1517–1721.
[10] E. Cerasi, R. Luft, S. Efendic, Decreased sensitivity of the pancreatic beta cells to glucose in prediabetic and diabetic subjects, a glucose dose–response study, Diabetes 21 (1972) 224–234.
[11] J. Eriksson, A. Franssila-Kallunki, A. Ekstrand, C. Saloranta, E. Widen, C. Schalin, et al., Early metabolic defects in persons at increased risk for non-insulin-dependent diabetes mellitus, N. Engl. J. Med. 321 (1989) 337–343.
[12] K. Matsumoto, S. Miyake, M. Yano, Y. Ueki, Y. Yamaguchi, S. Akazawa, et al., Glucose tolerance, insulin secretion, and insulin sensitivity in nonobese and obese Japanese subjects, Diabetes Care 20 (1997) 1562–1568.
[13] T. Kadowaki, Y. Miyake, R. Hagura, Y. Akanuma, H. Kajinuma, N. Kuzuya, et al., Risk factors for worsening to diabetes in subjects with impaired glucose tolerance, Diabetologia 26 (1984) 44–49.
[14] H.E. Lebovitz, Insulin secretagogues: old and new, Diabetes Review 7 (1999) 139–153.
[15] A. Bagust, S. Beale, Deteriorating beta-cell function in type 2 diabetes: a long-term model, QJM 96 (2003) 281–288.
[16] C.J. Rhodes, Type 2 diabetes—a matter of β-cell life and death? Science 307 (2005) 380–384.
[17] A.E. Butler, J. Janson, S. Bonner-Weir, R. Ritzel, R.A. Rizza, P.C. Butler, β-Cell deficit and increased β-cell apoptosis in humans with type 2 diabetes, Diabetes 52 (2003) 102–110.
[18] H. Sakuraba, H. Mizukami, N. Yagihashi, R. Wada, C. Hanyu, S. Yagihashi, Reduced beta-cell mass and expression of oxidative stress-related DNA damage in the islet of Japanese type II diabetic patients, Diabetologia 45 (2002) 85–96.
[19] K.H. Yoon, S.H. Ko, J.H. Cho, J.M. Lee, Y.B. Ahn, K.H. Song, et al., Selective beta-cell loss and alpha-cell expansion in patients with type 2 diabetes mellitus in Korea, J. Clin. Endocrinol. Metab. 88 (2003) 2300–2308.
[20] M.Y. Donath, P.A. Halban, Decreased beta-cell mass in diabetes: significance, mechanisms and therapeutic implications, Diabetologia 47 (2004) 581–589.
[21] D.T. Finegood, B.G. Topp, β-Cell deterioration-prospects for reversal or prevention, Diabetes Obes. Metab. 3 (Suppl. 1) (2001) S20–S27.
[22] M. Prentki, C.J. Nolan, Islet β cell failure in type 2 diabetes, J. Clin. Invest. 116 (2006) 1802–1812.
[23] A. Taniguchi, M. Fukushima, M. Saki, K. Kataoka, I. Nagata, K. Doi, et al., The role of the body mass index and triglyceride levels in identifying insulin-sensitive and insulin-resistant variants in Japanese non-insulin-dependent diabetic patients, Metabolism 49 (2000) 1001–1005.

Biochemical and Biophysical Research Communications 376 (2008) 21–25

Contents lists available at ScienceDirect

Biochemical and Biophysical Research Communications

journal homepage: www.elsevier.com/locate/ybbrc

Inhibition of GIP signaling modulates adiponectin levels under high-fat diet in mice

Rei Naitoh [a], Kazumasa Miyawaki [a], Norio Harada [a], Wataru Mizunoya [b], Kentaro Toyoda [a], Tohru Fushiki [b], Yuichiro Yamada [a,c], Yutaka Seino [a,d], Nobuya Inagaki [a,e,*]

[a] Department of Diabetes and Clinical Nutrition, Graduate School of Medicine, Kyoto University, 54 Shogoin Kawahara-cho, Sakyo-ku, Kyoto 606-8507, Japan
[b] Division of Food Science and Biotechnology, Graduate School of Agriculture, Kyoto University, Kyoto, Japan
[c] Department of Endocrinology and Diabetes and Geriatric Medicine, Akita University School of Medicine, Akita, Japan
[d] Kansai Electric Power Hospital, Osaka, Japan
[e] CREST of Japan Science and Technology Cooperation (JST), Kyoto, Japan

ARTICLE INFO

Article history:
Received 8 August 2008
Available online 22 August 2008

Keywords:
GIP
Fat oxidation
Adiponectin
PPAR

ABSTRACT

Gastric inhibitory polypeptide (GIP) is an incretin and directly promotes fat accumulation in adipocytes. Inhibition of GIP signaling prevents onset of obesity and increases fat oxidation in peripheral tissues under high-fat diet (HFD), but the mechanism is unknown. In the present study, we investigated the effects of inhibition of GIP signaling on adiponectin levels after 3 weeks of HFD by comparing wild-type (WT) mice and GIP receptor-deficient ($Gipr^{-/-}$) mice. In HFD-fed $Gipr^{-/-}$ mice, fat oxidation was significantly increased and adiponectin mRNA levels in white adipose tissue and plasma adiponectin levels were significantly increased compared to those in HFD-fed WT mice. In addition, the PPARα mRNA level was increased and the ACC mRNA level was decreased in skeletal muscle of HFD-fed $Gipr^{-/-}$ mice compared with those in HFD-fed WT mice. These results indicate that inhibition of GIP signaling increases adiponectin levels, resulting in increased fat oxidation in peripheral tissues under HFD.

Gastric inhibitory polypeptide (GIP) is a major incretin that potentiates insulin secretion in pancreatic β-cells in the presence of glucose [1,2]. GIP is released from duodenal endocrine K-cells after meal ingestion, and acts by binding the GIP receptor through increased intracellular cAMP [3]. The GIP receptor is expressed in pancreas, stomach, small intestine, heart, adrenal cortex, brain, lung, bone, vascular endothelium, and adipose tissue [4]. In addition to the insulinotropic effects on pancreatic β-cells, GIP is an obesity-promoting factor that directly leads to the accumulation of fat in adipocytes. In vitro studies show that GIP stimulates synthesis and secretion of lipoprotein lipase (LPL) in cultured preadipocytes [5], and that GIP promotes LPL activity in fat tissue [6]. It also has been shown that GIP stimulates glucose transport and increases fatty-acid synthesis in fat tissue [7]. Studies of GIP receptor-deficient mice ($Gipr^{-/-}$ mice) show that GIP also is an important factor in the promotion of obesity in vivo [8]. High-fat diet (HFD)-fed wild-type (WT) mice exhibit body weight gain and markedly increased visceral and subcutaneous fat mass and liver steatosis. By contrast, $Gipr^{-/-}$ mice fed HFD exhibit neither weight gain nor adiposity. Furthermore, measurement of the respiratory quotient reveals that fat is used as the preferred energy substrate in $Gipr^{-/-}$ mice. In addition, a study using IRS-$1^{-/-}$/$Gipr^{-/-}$ double-deficient mice demonstrated that inhibition of GIP signaling increases fatty-acid oxidation in peripheral tissues under diminished insulin signaling [9]. Thus, GIP plays a critical role in adiposity, but the mechanism of fat oxidation in peripheral tissues in the absence of GIP signaling is unclear.

Adiponectin is one of the major adipokines secreted from adipocytes, and stimulates fat oxidation in peripheral tissues. Adiponectin promotes AMPK activation and PPARα expression and stimulates fat oxidation in skeletal muscle and liver [10]. In the present study, we investigated the effects of the inhibition of GIP signaling on adiponectin levels and the stimulation of fat oxidation that averts obesity by comparing WT mice and $Gipr^{-/-}$ mice fed HFD. To clarify the early response to HFD-induced obesity, we performed the experiments on mice at 3 weeks of HFD and control-fat diet (CD).

Materials and methods

Animals. The generation of $Gipr^{-/-}$ mice (C57BL/6 background) has been described previously [11]. At 7 weeks of age, WT and $Gipr^{-/-}$ mice were fed HFD or CD for 7 weeks. HFD supplied 45% of calories as fat, 35% as carbohydrate, and 20% as protein, with energy density of 3.57 kcal/g. CD supplied 13% of calories as fat, 60% as carbohydrate, and 27% as protein, with energy density of

* Corresponding author. Address: Department of Diabetes and Clinical Nutrition, Graduate School of Medicine, Kyoto University, 54 Shogoin Kawahara-cho, Sakyo-ku, Kyoto 606-8507, Japan. Fax: +81 75 751 4244.
E-mail address: inagki@metab.kuhp.kyoto-u.ac.jp (N. Inagaki).

0006-291X/$ - see front matter © 2008 Elsevier Inc. All rights reserved.
doi:10.1016/j.bbrc.2008.08.052

3.57 kcal/g. Animal care and procedures were approved by the Animal Care Committee of Kyoto University.

Energy expenditure. Energy expenditure was evaluated by measuring respiratory quotient and oxygen consumption by indirect calorimetry every 13 min for 24 h in mice under the fed condition, as described previously [8,9,12]. Air from the room was pumped through the chamber, and expired gas was dried in a cotton thin column and subjected to gas analysis (Alco System model RL-600, Chiba, Japan). O_2 and CO_2 concentrations were measured, and oxygen consumption (VO_2), carbon dioxide exhaustion (VCO_2), respiratory quotient (RQ), and fat oxidation were calculated as described previously [12].

Computed tomography. Mice were anesthetized with pentobarbital and fixed in a chamber, and transaxially scanned using Latheta (LCT-100M) experimental animal CT system (Aloka, Tokyo, Japan). The whole body was scanned, and contiguous 1-mm slice images of the trunk were used for quantitative assessment (Latheta software, version 1.00). Weight of visceral fat mass and lean mass were quantitatively evaluated.

Measurement of plasma adiponectin levels and Western blot analysis. Blood samples were collected from the tail vein at the end of the dark phase and centrifuged (3000 rpm, 10 min, 4 °C). Levels of plasma adiponectin were measured using an adiponectin ELISA kit (Otsuka, Tokyo, Japan).

Plasma samples of HFD-fed mice were subjected to SDS–PAGE using Laemmli's method [13]. SDS–PAGE was performed under non-reducing and non-heat-denaturing conditions, as previously reported [14]. Western blot analysis was performed using anti-mouse adiponectin antibody. Densities of corresponding bands were quantified by NIH-Image.

Isolation of total RNA and quantitative RT-PCR. Total RNA was isolated from muscle and white adipose tissue (epididymal fat pad, (WAT)) using Trizol (Invitrogen, Grand Island, NY). mRNA levels were measured by real-time quantitative RT-PCR using ABI PRISM 7000 Sequence Detection System (Applied Biosystems, Foster City, CA). mRNA levels were corrected for GAPDH (Applied Biosystems) mRNA level. Sequences of PPARα primers were 5′-CGACCTGAAAG ATTCGGAAA-3′ and 5′-CCTCTGCCTCTTTGTCTTC-3′; sequences of ACC primers were 5′-CCTCCGAGGAACCCTCTGT-3′ and 5′-CGGCTGT CCAGTTGGTTTG-3′; sequences of adiponectin primers were 5′-G GAACTTGTGCAGGTTGGAT-3′ and 5′-GCTTCTCCAGGCTCTCCTTT-3′; and sequences of PPARγ primers were 5′-TGTCGGTTTCAGAAGT GCCTT-3′ and 5′-GCTCGCAGATCAGCAGACTCT-3′.

Statistical analysis. Data are expressed as means ± SE. Statistical analysis was performed by ANOVA and unpaired student's test. P values <0.05 were considered significant.

Results

Body weight and fat mass in HFD-fed Gipr$^{-/-}$ mice

WT mice exhibited significant weight gain after 3 weeks of HFD feeding (Fig. 1A). By contrast, body weight of HFD-fed Gipr$^{-/-}$ mice was not increased compared with that of CD-fed Gipr$^{-/-}$ mice after 3 weeks of study (Fig. 1B). The lesser body weight of Gipr$^{-/-}$ mice continued through 7 weeks of HFD feeding.

At the early stage of 3 weeks of HFD feeding, CT analysis was performed to estimate visceral fat mass in WT and Gipr$^{-/-}$ mice. There was no significant difference in visceral fat mass between WT and Gipr$^{-/-}$ mice under CD feeding. Visceral fat mass of HFD-fed WT and Gipr$^{-/-}$ mice were significantly increased compared with those of CD-fed WT and Gipr$^{-/-}$ mice by 100% and 52%, respectively. In HFD-fed mice, visceral fat mass of WT mice was significantly increased compared with that of Gipr$^{-/-}$ mice (Fig. 1C and D). There was no difference in lean body mass (data not shown). There also was no difference in food intake between WT and Gipr$^{-/-}$ mice (data not shown).

Fat consumption in HFD-fed Gipr$^{-/-}$ mice

To evaluate energy consumption in the early stage of HFD feeding, respiratory quotient and oxygen consumption were measured

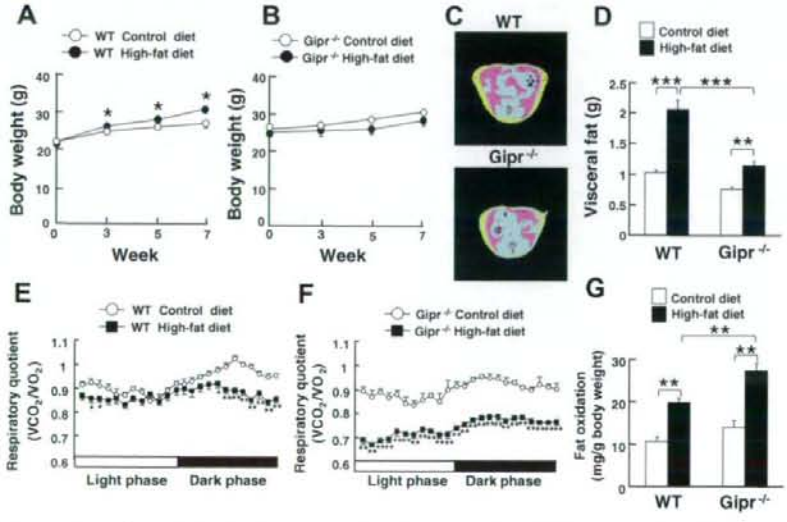

Fig. 1. Body weight in WT mice (A) and Gipr$^{-/-}$ mice (B) during 7 weeks on CD (open circles) and HFD (filled circles). (C) CT-based body composition analysis. WT mice and Gipr$^{-/-}$ mice at 3 weeks on HFD feeding. Representative CT images were taken at the same slice level. Pink, yellow, and blue areas represent visceral fat, subcutaneous fat, and lean mass. (D) Visceral fat accumulation in WT mice and Gipr$^{-/-}$ mice at 3 weeks on CD (open bars) and HFD (filled bars). Respiratory quotient in WT mice (E) and Gipr$^{-/-}$ mice (F) at 3 weeks on CD (open circles) and HFD (filled square). (G) Calculated fat oxidation in WT mice and Gipr$^{-/-}$ mice at 3 weeks on CD (open bars) and HFD (filled bars). n = 5–12. Values are means ± SE. $^{*}P < 0.05$, $^{**}P < 0.01$, $^{***}P < 0.005$. (For interpretation of the references to color in this figure legend, the reader is referred to the web version of this paper.)

by indirect calorimetry. HFD-fed WT mice exhibited a significant reduction of respiratory quotient only in part of the dark phase compared with CD-fed WT mice (Fig. 1E). By contrast, HFD-fed Gipr$^{-/-}$ mice exhibited a significant reduction of respiratory quotient throughout the day compared with CD-fed Gipr$^{-/-}$ mice (Fig. 1F). At 3 weeks of HFD feeding, calculated fat oxidation was significantly increased in Gipr$^{-/-}$ mice compared with that in WT mice (Fig. 1G). These results indicate that Gipr$^{-/-}$ mice use fat as preferred energy substrate in the early stage of HFD feeding.

Adiponectin levels of Gipr$^{-/-}$ mice in the early stage of HFD feeding

We examined mRNA expression level of adiponectin in white adipose tissue (WAT) and plasma adiponectin levels in Gipr$^{-/-}$ mice. mRNA expression of adiponectin in WAT and plasma adiponectin levels were significantly increased in HFD-fed Gipr$^{-/-}$ mice compared with those in HFD-fed WT mice (Fig. 2A and B). In addition, in Gipr$^{-/-}$ mice, mRNA expression level of adiponectin in WAT and plasma adiponectin levels were significantly increased in HFD-fed mice compared with those in CD-fed mice, although HFD feeding decreased mRNA expression of adiponectin and plasma adiponectin levels in WT mice (Fig. 2A and B).

To determine qualitative differences in adiponectin, we performed Western blot analysis. Levels of middle molecular weight (MMW) and low molecular weight (LMW) multimers of adiponectin were significantly higher in HFD-fed Gipr$^{-/-}$ mice compared to those in HFD-fed WT mice (Fig. 2C and Table 1). There were no significant differences in high molecular weight multimers (HMW) of adiponectin between HFD-fed WT and Gipr$^{-/-}$ mice.

As PPARγ (peroxisome proliferator-activated receptor-γ) is known to be involved in the regulation of adiponectin, we examined mRNA expression levels of PPARγ in WAT. While HFD-fed WT mice showed a tendency to decreased mRNA expression of PPARγ, the mRNA expression level of PPARγ was significantly increased in HFD-fed Gipr$^{-/-}$ mice compared with that in HFD-fed WT mice (Fig. 2D). These results suggest that inhibition of GIP signaling modulates adiponectin levels through PPARγ.

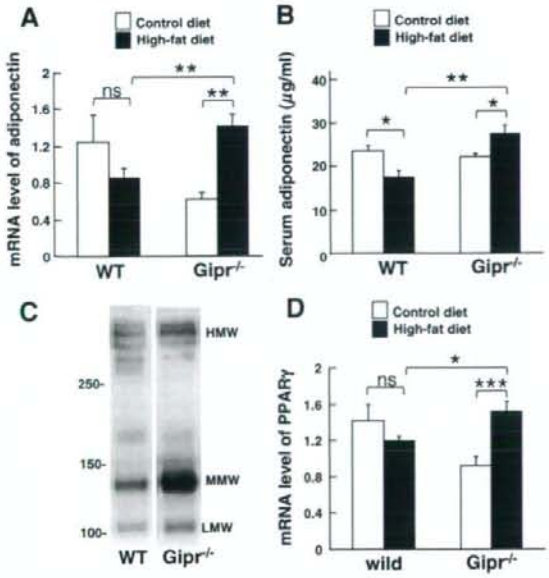

Fig. 2. mRNA expression level of adiponectin in WAT (A) and plasma adiponectin level (B) at 3 weeks on CD (open bars) and HFD (filled bars). $n = 7$–8 mice/group. Values are means ± SE. $^{*}P < 0.05$, $^{**}P < 0.01$. (C) Non-reducing and non-heat-denaturing SDS–PAGE of adiponectin in WT mice and Gipr$^{-/-}$ mice at 3 weeks on HFD. (D) mRNA expression level of PPARγ in WAT at 3 weeks on CD (open bars) and HFD (filled bars). $n = 4$–7. Values are means ± SE. $^{*}P < 0.05$, $^{***}P < 0.005$. ns, not significant.

Table 1
Difference in multimer formation of adiponectin in WT mice and Gipr$^{-/-}$ mice at 3 weeks on high-fat diet

	WT	Gipr$^{-/-}$
HMW	100 ± 22.0	131.9 ± 17.8
MMW	100 ± 9.1	154.3 ± 5.9*
LMW	100 ± 13	163.4 ± 15.3*

Values for Gipr$^{-/-}$ mice represent relative density (%) regarding average value for WT mice as 100. $n = 5$. Values are means ± SE.
* $P < 0.05$ vs. WT mice.

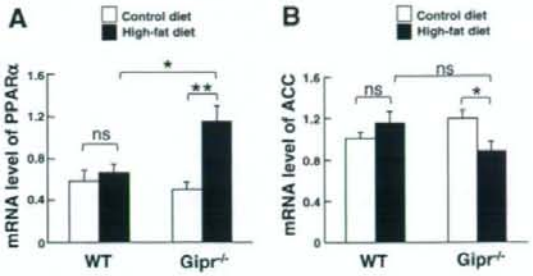

Fig. 3. mRNA expression level of PPARα (A) and ACC (B) in skeletal muscle at 3 weeks on CD (open bars) and HFD (filled bars). $n = 5$–7. Values are means ± SE. $^{*}P < 0.05$, $^{**}P < 0.01$. ns, not significant.

Expression levels of PPARα and ACC mRNAs in skeletal muscle of Gipr$^{-/-}$ mice at the early stage of HFD feeding

To determine the effects of adiponectin on peripheral tissues in the absence of GIP signaling, mRNA expression levels of PPARα (peroxisome proliferator-activated receptor-α) and ACC (acetyl-CoA carboxylase) in skeletal muscle and liver were examined. mRNA expression level of PPARα mRNA was significantly increased in HFD-fed Gipr$^{-/-}$ mice compared with that in CD-fed Gipr$^{-/-}$ mice in skeletal muscle (Fig. 3A). Although there was no significant difference in phosphorylation of AMPK (AMP-activated protein kinase) between HFD-fed WT and Gipr$^{-/-}$ mice by western blot analysis (data not shown), mRNA expression level of ACC, which is inactivated by AMPK, was significantly reduced in muscle of HFD-fed Gipr$^{-/-}$ mice compared with that in CD-fed Gipr$^{-/-}$ mice (Fig. 3B). These results indicate that fat oxidation is increased in skeletal muscle of Gipr$^{-/-}$ mice in the early stage of HFD feeding. We also examined mRNA expression levels of PPARα and ACC in liver, but no significant differences were found among the groups of mice (data not shown).

Discussion

In this study, we investigated the effects of GIP inhibition on fat oxidation in the early stage (3 weeks) of HFD feeding, and found that inhibition of GIP signaling increases the level of adiponectin, which promotes fat oxidation in peripheral tissues.

The GIP receptor is expressed in adipocytes as well as in pancreatic β-cells, and GIP signaling directly promotes energy accumulation into adipocytes. Previously, Gipr$^{-/-}$ mice were shown to exhibit resistance to high-fat-induced obesity, and to use fat as the preferred energy substrate [8]. In that study, mice were fed

HFD for a long period of from 7 to 50 weeks of age. In the present study, we investigated HFD-fed mice in the short, early period from 7 to 10 weeks of age, and found Gipr$^{-/-}$ mice to be resistant to obesity as well as to accumulation of visceral fat, and that fat oxidation was significantly increased, demonstrating that GIP plays a critical role in promoting obesity even at 3 weeks on HFD feeding.

Leptin and adiponectin are major adipokines that activate fat oxidation for body weight control. They affect AMPK activation and stimulate fat oxidation in skeletal muscle and liver [10,15]. It has been reported that inhibition of GIP signaling decreases body weight even in leptin-deficient ob/ob mice [8], indicating that factors other than leptin increase fat oxidation under conditions of inhibited GIP signaling. Leptin suppresses food intake through the central nervous system, and there were no differences in food intake between WT and Gipr$^{-/-}$ mice in CD-fed and HFD-fed mice in the present study. Thus, we focused on adiponectin, and hypothesized that inhibition of GIP signaling modulates adiponectin levels and affects on fat oxidation in peripheral tissues. The mRNA expression level of adiponectin in adipocytes and adiponectin concentrations in plasma are reduced in obese and insulin-resistant states which increases visceral fat mass [16,17]. In the present study, mRNA expression level of adiponectin in WAT and plasma adiponectin levels were found to be decreased and visceral fat mass was increased in HFD-fed WT mice compared with CD-fed WT mice. The mRNA expression and plasma levels of adiponectin were significantly increased in HFD-fed Gipr$^{-/-}$ mice compared with those in CD-fed Gipr$^{-/-}$ mice, although visceral fat mass of HFD-fed Gipr$^{-/-}$ mice was significantly increased compared with that of CD-fed Gipr$^{-/-}$ mice. These results suggest that GIP may reduce adiponectin levels in adipocytes. It has been previously reported that Gipr$^{-/-}$ mice show no difference in plasma adiponectin levels between CD-fed and HFD-fed mice after a long period of 20 weeks, when obesity is established [18]. On the other hand, we measured adiponectin levels of mice fed HFD for a short period of 3 weeks, and demonstrate that inhibition GIP signaling modulates adiponectin even in the very early stage when obesity first begins to appear in WT mice.

While skeletal muscle and liver are the major sites of body fat oxidation, the GIP receptor is not expressed in these tissues. PPARα and AMPK are the most important molecules in the control of fat oxidation in muscle and liver. Adiponectin increases expression levels of PPARα and induces phosphorylation of AMPK [16,19]. AMPK activated by adiponectin suppresses ACC activity, which catalyses the formation of malonyl-CoA and stimulates fat oxidation [20]. We found that the mRNA expression level of PPARα was significantly increased and that of ACC was significantly reduced in skeletal muscle of HFD-fed Gipr$^{-/-}$ mice compared to those in CD-fed Gipr$^{-/-}$ mice. These results indicate that fat oxidation is increased in skeletal muscle of Gipr$^{-/-}$ mice in the early stage of HFD feeding, but there was no significant difference in liver. Adiponectin has three forms: trimers (low molecular weight, LMW), hexamers (middle molecular weight, MMW), and multimers (high molecular weight, HMW), and differing tissue-specific effects of these forms on AMPK phosphorylation have been reported [21]. Only trimers activate AMPK in muscle; hexamers and the high molecular isoform do not [22]. It also has been reported that trimers are the most potent isoform in skeletal muscle [19,23]. The trimer isoform of adiponectin was found in the present study to be significantly increased in HFD-fed Gipr$^{-/-}$ mice. This finding may explain the difference of PPARα and ACC expression between skeletal muscle and liver in HFD-fed Gipr$^{-/-}$ mice.

In conclusion, we show that inhibition of GIP signaling upregulates the adiponectin level and increases fat oxidation in skeletal muscle. These findings suggest that the influence of GIP on adiposity is, at least in part, mediated by modulation of adiponectin expression in adipocytes in the early stage of HFD feeding.

Acknowledgments

We thank Drs. Takashi Kadowaki and Naoto Kubota (Department of Diabetes and Metabolic Disease, Tokyo University Graduate School of Medicine) for providing anti-mouse adiponectin antibody and for their valuable suggestion.

We also thank Drs. Katsushi Tsukiyama, Rie Watanabe, Heying Zhou, Chizumi Yamada, and Yukiko Kawasaki for their technical help and for their valuable comments.

This study was supported by Scientific Research Grants from the Ministry of Education, Culture, Sports, Science, and Technology, Japan, and from the Ministry of Health, Labor, and Welfare, Japan.

References

[1] P. Schauder, J. Brown, H. Frerichs, W. Creutzfeldt, Gastric inhibitory polypeptide: effect on glucose-induced insulin release from isolated rat pancreatic islets in vitro, Diabetologia 11 (1975) 483–484.
[2] J. Dupre, S. Ross, D. Watson, J. Brown, Stimulation of insulin secretion by gastric inhibitory polypeptide in man, J. Clin. Endocrinol. Metab. 37 (1973) 826–828.
[3] Y. Yamada, K. Miyawaki, K. Tsukiyama, N. Harada, C. Yamada, Y. Seino, Pancreatic and extrapancreatic effects of gastric inhibitory polypeptide, Diabetes 55 (Suppl. 2) (2006) S86–S91.
[4] T.B. Usdin, E. Mezey, D.C. Button, M.J. Brownstein, T.I. Bonner, Gastric inhibitory polypeptide receptor, a member of the secretin-vasoactive intestinal peptide receptor family, is widely distributed in peripheral organs and the brain, Endocrinology 133 (1993) 2861–2870.
[5] R.H. Eckel, W.Y. Fujimoto, J.D. Brunzell, Gastric inhibitory polypeptide enhanced lipoprotein lipase activity in cultured preadipocytes, Diabetes 28 (1979) 1141–1142.
[6] J. Knapper, S. Puddicombe, L. Morgan, J. Fletcher, Investigations into the actions of glucose-dependent insulinotropic polypeptide and glucagon-like peptide-1(7-36)amide on lipoprotein lipase activity in explants of rat adipose tissue, J. Nutr. 125 (1995) 183–188.
[7] H. Hauner, G. Glatting, D. Kaminska, E. Pfeiffer, Effects of gastric inhibitory polypeptide on glucose and lipid metabolism of isolated rat adipocytes, Ann. Nutr. Metab. 32 (1988) 282–288.
[8] K. Miyawaki, Y. Yamada, N. Ban, Y. Ihara, K. Tsukiyama, H. Zhou, S. Fujimoto, A. Oku, K. Tsuda, S. Toyokuni, H. Hiai, W. Mizunoya, T. Fushiki, J. Holst, M. Makino, A. Tashita, Y. Kobara, Y. Tsubamoto, T. Jinnouchi, T. Jomori, Y. Seino, Inhibition of gastric inhibitory polypeptide signaling prevents obesity, Nat. Med. 8 (2002) 738–742.
[9] H. Zhou, Y. Yamada, K. Tsukiyama, K. Miyawaki, M. Hosokawa, K. Nagashima, K. Toyoda, R. Naitoh, W. Mizunoya, T. Fushiki, T. Kadowaki, Y. Seino, Gastric inhibitory polypeptide modulates adiposity and fat oxidation under diminished insulin action, Biochem. Biophys. Res. Commun. 335 (2005) 937–942.
[10] T. Kadowaki, T. Yamauchi, Adiponectin and adiponectin receptors, Endocr. Rev. 26 (2005) 439–451.
[11] K. Miyawaki, Y. Yamada, H. Yano, H. Niwa, N. Ban, Y. Ihara, A. Kubota, S. Fujimoto, M. Kajikawa, A. Kuroe, K. Tsuda, H. Hashimoto, T. Yamashita, T. Jomori, F. Tashiro, J. Miyazaki, Y. Seino, Glucose intolerance caused by a defect in the entero-insular axis: a study in gastric inhibitory polypeptide receptor knockout mice, Proc. Natl. Acad. Sci. USA 96 (1999) 14843–14847.
[12] K. Ishihara, S. Oyaizu, K. Onuki, K. Lim, T. Fushiki, Chronic (−)-hydroxycitrate administration spares carbohydrate utilization and promotes lipid oxidation during exercise in mice, J. Nutr. 130 (2000) 2990–2995.
[13] U.K. Laemmli, Cleavage of structural proteins during the assembly of the head of bacteriophage T4, Nature 227 (1970) 680–685.
[14] H. Waki, T. Yamauchi, J. Kamon, Y. Ito, S. Uchida, S. Kita, K. Hara, Y. Hada, F. Vasseur, P. Froguel, S. Kimura, R. Nagai, T. Kadowaki, Impaired multimerization of human adiponectin mutants associated with diabetes. Molecular structure and multimer formation of adiponectin, J. Biol. Chem. 278 (2003) 40352–40363.
[15] Y. Minokoshi, Y. Kim, O. Peroni, L. Fryer, C. Müller, D. Carling, B. Kahn, Leptin stimulates fatty-acid oxidation by activating AMP-activated protein kinase, Nature 415 (2002) 339–343.
[16] T. Yamauchi, J. Kamon, H. Waki, Y. Imai, N. Shimozawa, K. Hioki, S. Uchida, Y. Ito, K. Takakuwa, J. Matsui, M. Takata, K. Eto, Y. Terauchi, K. Komeda, M. Tsunoda, K. Murakami, Y. Ohnishi, T. Naitoh, K. Yamamura, Y. Ueyama, P. Froguel, S. Kimura, R. Nagai, T. Kadowaki, Globular adiponectin protected ob/ob mice from diabetes and ApoE-deficient mice from atherosclerosis, J. Biol. Chem. 278 (2003) 2461–2468.
[17] C. Weyer, T. Funahashi, S. Tanaka, K. Hotta, Y. Matsuzawa, R. Pratley, P. Tataranni, Hypoadiponectinemia in obesity and type 2 diabetes: close association with insulin resistance and hyperinsulinemia, J. Clin. Endocrinol. Metab. 86 (2001) 1930–1935.
[18] T. Hansotia, A. Maida, G. Flock, Y. Yamada, K. Tsukiyama, Y. Seino, D.J. Drucker, Extrapancreatic incretin receptors modulate glucose homeostasis, body weight, and energy expenditure, J Clin Invest 117 (2007) 143–152.
[19] T. Yamauchi, J. Kamon, H. Waki, Y. Terauchi, N. Kubota, K. Hara, Y. Mori, T. Ide, K. Murakami, N. Tsuboyama-Kasaoka, O. Ezaki, Y. Akanuma, O. Gavrilova, C.

Vinson, M. Reitman, H. Kagechika, K. Shudo, M. Yoda, Y. Nakano, K. Tobe, R. Nagai, S. Kimura, M. Tomita, P. Froguel, T. Kadowaki, The fat-derived hormone adiponectin reverses insulin resistance associated with both lipoatrophy and obesity, Nat. Med. 7 (2001) 941–946.
[20] B. Kiens, Skeletal muscle lipid metabolism in exercise and insulin resistance, Physiol. Rev. 86 (2006) 205–243.
[21] M. Barnea, A. Shamay, A. Stark, Z. Madar, A high-fat diet has a tissue-specific effect on adiponectin and related enzyme expression, Obesity (Silver Spring) 14 (2006) 2145–2153.
[22] T. Tsao, E. Tomas, H. Murrey, C. Hug, D. Lee, N. Ruderman, J. Heuser, H. Lodish, Role of disulfide bonds in Acrp30/adiponectin structure and signaling specificity. Different oligomers activate different signal transduction pathways, J. Biol. Chem. 278 (2003) 50810–50817.
[23] J. Fruebis, T. Tsao, S. Javorschi, D. Ebbets-Reed, M. Erickson, F. Yen, B. Bihain, H. Lodish, Proteolytic cleavage product of 30-kDa adipocyte complement-related protein increases fatty acid oxidation in muscle and causes weight loss in mice, Proc. Natl. Acad. Sci. USA 98 (2001) 2005–2010.

Am J Physiol Lung Cell Mol Physiol 295: L698–L707, 2008.
First published August 1, 2008; doi:10.1152/ajplung.90352.2008.

Aberrant catalytic cycle and impaired lipid transport into intracellular vesicles in ABCA3 mutants associated with nonfatal pediatric interstitial lung disease

Yoshihiro Matsumura,[1] Nobuhiro Ban,[1,2] and Nobuya Inagaki[1,2]

[1]*Department of Physiology, Akita University School of Medicine, Akita; and* [2]*Department of Diabetes and Clinical Nutrition, Graduate School of Medicine, Kyoto University, and Core Research for Evolutional Science and Technology of Japan Science and Technology Agency, Kyoto, Japan*

Submitted 18 June 2008; accepted in final form 31 July 2008

Matsumura Y, Ban N, Inagaki N. Aberrant catalytic cycle and impaired lipid transport into intracellular vesicles in ABCA3 mutants associated with nonfatal pediatric interstitial lung disease. *Am J Physiol Lung Cell Mol Physiol* 295: L698–L707, 2008. First published August 1, 2008; doi:10.1152/ajplung.90352.2008.—The ATP-binding cassette transporter ABCA3 mediates uptake of choline-phospholipids into intracellular vesicles and is essential for surfactant metabolism in lung alveolar type II cells. We have shown previously that *ABCA3* mutations in fatal surfactant deficiency impair intracellular localization or ATP hydrolysis of ABCA3 protein. However, the mechanisms underlying the less severe phenotype of patients with *ABCA3* mutation are unclear. In this study, we characterized ABCA3 mutant proteins identified in pediatric interstitial lung disease (pILD). E292V (intracellular loop 1), E690K (adjacent to Walker B motif in nucleotide binding domain 1), and T1114M (8th putative transmembrane segment) mutant proteins are localized mainly in intracellular vesicle membranes as wild-type protein. Lipid analysis and sucrose gradient fractionation revealed that the transport function of E292V mutant protein is moderately preserved, whereas those of E690K and T1114M mutant proteins are severely impaired. Vanadate-induced nucleotide trapping and photoaffinity labeling of wild-type and mutant proteins using 8-azido-[^{32}P]ATP revealed an aberrant catalytic cycle in these mutant proteins. These results demonstrate the importance of a functional catalytic cycle in lipid transport of ABCA3 and suggest a pathophysiological mechanism of pILD due to *ABCA3* mutation.

ATP-binding cassette A3 mutant; pediatric interstitial lung disease; lamellar body; lipid transporter; phosphatidylcholine

THE FAMILY OF ATP-BINDING CASSETTE (ABC) transporters is involved in ATP-dependent transport of various substrates across membranes (14). ABCA3 is expressed predominantly at the limiting membrane of the lamellar bodies in lung alveolar type II cells and is proposed to be a surfactant lipid transporter (20, 36). Exogenous expression of ABCA3 in cultured cells promotes lipid uptake into intracellular vesicles that generate lamellar body-like vesicles (7, 18, 21). ABCA3 deficiency in human and mice leads to decreased phosphatidylcholine and phosphatidylglycerol in surfactant, dysgenesis of lamellar bodies, and respiratory distress (1, 3, 8, 11, 12, 27). Considered together, these results indicate that ABCA3 is an essential lipid transporter in surfactant metabolism.

In addition, *ABCA3* mutations cause lung disease of differing severity. We previously found that *ABCA3* mutations in fatal surfactant deficiency can result in abnormal intracellular localization (type I) or impaired ATP hydrolysis of ABCA3 protein (type II) (17). For example, patients with type I homozygous *ABCA3* mutations such as W1142X/W1142X or type I/type II compound heterozygous *ABCA3* mutations such as L982P/G1221S die of surfactant deficiency within the neonatal period (27). On the other hand, patients with the common missense mutation E292V and a second, specific mutation such as E690K or T1114M develop pediatric interstitial lung disease (pILD), the phenotype of which is milder than that of fatal surfactant deficiency, suggesting that the E292V *ABCA3* mutation is responsible for the development of pILD (4). However, the mechanism underlying the phenotypic heterogeneity of lung disease associated with *ABCA3* mutation remains unknown.

In this study, we characterized E292V, E690K, and T1114M mutant ABCA3 proteins identified in pILD. Analysis of these ABCA3 mutants demonstrates the importance of a functional catalytic cycle in the lipid transport function of ABCA3 and suggests various therapeutic targets in lung disease due to *ABCA3* mutation.

MATERIALS AND METHODS

DNA construction. The plasmid pEGFPN1-ABCA3 (17), which encodes ABCA3 protein fused with enhanced green fluorescent protein (GFP) at the COOH terminus (ABCA3-GFP), and its mutants containing pILD mutations (E292V, E690K, and T1114M) and other site-directed mutations (E292D, E292K, T1114S, E690D, and E690R) were generated as described previously and used for transient transfection experiment. Plasmid pCAGIpuro-ABCA3-GFP (17), which encodes ABCA3-GFP and its mutants described above, driven by a CAG promoter containing an internal ribosomal entry site and puromycin *N*-acetyltransferase gene cassette (22), was generated as described previously and used for stable transfection experiments.

Confocal microscopy. Human embryonic kidney (HEK-293) cells were grown at 37°C under 5% CO_2 in Dulbecco's modified Eagle's medium (Sigma) supplemented with 10% fetal calf serum and penicillin/streptomycin. HEK-293 cells (3×10^5) were seeded into 35-mm dishes with a poly-L-lysine-coated cover glass. After 24 h, HEK-293 cells were transfected with wild-type or mutant pEGFP plasmid (1 μg) using FuGENE transfection reagent (Roche Applied Science). The transfected cells were cultured for 48 h, fixed with 4% paraformaldehyde, and viewed with a Zeiss confocal microscope LSM510-META.

Glycosylation of ABCA3-GFP and mutant proteins. HEK-293 cells (3×10^6) were seeded into 100-mm dishes 24 h before transfection. Forty-eight hours after transfection with pEGFP vectors (6.25 μg) using FuGENE reagent, the cells were homogenized in 50 mM Tris·HCl buffer (pH 7.5) containing Complete protease inhibitor mixture (Roche Applied Science), and the total membrane fraction

Address for reprint requests and other correspondence: N. Inagaki, Dept. of Diabetes and Clinical Nutrition, Graduate School of Medicine, Kyoto Univ., 54 Kawahara-cho, Shogoin, Sakyo-ku, Kyoto 606-8507, Japan (e-mail: inagaki@metab.kuhp.kyoto-u.ac.jp).

The costs of publication of this article were defrayed in part by the payment of page charges. The article must therefore be hereby marked "*advertisement*" in accordance with 18 U.S.C. Section 1734 solely to indicate this fact.

(100,000-*g* pellet) was obtained as described previously (17). Ten micrograms of total membrane fraction were treated with 1 unit of peptide *N*-glycosidase F (PNGase F) or 5 milliunits of endoglycosidase H (Endo H) for 30 min at 37°C. The deglycosylated proteins were separated by SDS-PAGE and analyzed by immunoblot analysis using anti-GFP monoclonal antibody (Santa Cruz Biotechnology).

Establishment of HEK-293 cells stably expressing ABCA3-GFP and mutant proteins. HEK-293 cells (3×10^5) were seeded into 35-mm dishes and, after 24 h, transfected with linearized pCAGIpuro plasmids (1 μg) with *PvuI* using FuGENE reagent. Forty-eight hours after transfection, the cells were trypsinized, seeded into 100-mm dishes, and selected by 2.5 μg/ml puromycin for 7 days. Resistant colonies were combined and used for lipid analysis, whereas single colonies were isolated and used for nucleotide trapping and photoaffinity labeling experiments. The expression of ABCA3-GFP, LAMP3, and GRP78 was examined by immunoblot analysis using anti-GFP, anti-LAMP3 (Chemicon), and anti-GRP78 (Santa Cruz Biotechnology) antibodies, respectively.

Sucrose gradient fractionation. Confluent cells (five 100-mm dishes) were harvested and disrupted in 20 mM Tris·HCl buffer (pH 7.3) containing 1 M sucrose and Complete protease inhibitor mixture by N_2 cavitation, followed by centrifugation at 1,000 *g* for 10 min to obtain postnuclear supernatant (PNS). A sucrose gradient consisting of 1 ml each of 0.8, 0.7, 0.6, 0.5, 0.4, and 0.3 M sucrose and 0.5 ml of 0.2 M sucrose was layered successively above 3.5 ml of PNS (4 mg of protein). The gradient was spun in a P40ST rotor (Hitachi) at 125 *g* for 15 min and then at 80,000 *g* for 3 h. After centrifugation, 1 ml of each fraction was collected from the top.

Lipids analysis. Total lipids in PNS and sucrose gradient fractions were extracted using the method of Bligh and Dyer (2). The amount of total cholesterol and choline-phospholipids was measured using an enzymatic assay kit (Kyowa Medex and Wako, respectively). Data normalized by the protein content are represented as means ± SD, and statistical analysis was performed using the Bonferroni/Dunn procedure for post hoc testing.

Vanadate-induced nucleotide trapping of ABCA3-GFP and mutant proteins. A 20,000-*g* membrane fraction was obtained from HEK-293 cells stably expressing wild-type ABCA3-GFP or mutants as described previously (17). A 20,000-*g* membrane fraction (18–24 μg of protein) was incubated with 10 μM 8-azido-[α-^{32}P]ATP, 2 mM ouabain, 0.1 mM EGTA, 3 mM $MgCl_2$, and 40 mM Tris·HCl (pH 7.5) in a total volume of 12 μl for 10 min at 37°C in the presence or absence of 0.4 mM orthovanadate. In some experiments, 8-azido-[α-^{32}P]ATP was replaced with 8-azido-[γ-^{32}P]ATP. The reaction was stopped by adding 400 μl of ice-cold TEM buffer [40 mM Tris·HCl buffer (pH 7.5) containing 0.1 mM EGTA and 1 mM $MgCl_2$]. The supernatant containing unbound nucleotides was removed from the membrane pellet after centrifugation (20,000 *g*, 10 min, 2°C), and the procedure was repeated once. In the release experiment, following the initial removal of unbound nucleotides, the pellets were suspended in 100 μl of TEM buffer and incubated for 0–15 min at 37°C to release trapped nucleotides. After incubation, 300 μl of TEM buffer were added and supernatant containing released nucleotides was removed from the membrane pellet after centrifugation (20,000 *g*, 10 min, 2°C). The pellets were resuspended in 10 μl of TEM buffer and irradiated for 5 min (254 nm, 8.2 mW/cm^2) on ice. The samples were then electrophoresed on a 5% SDS-polyacrylamide gel and transferred to a polyvinylidene difluoride (PVDF) membrane (Millipore). The radioactivities of photoaffinity-labeled protein (total 220-kDa noncleaved form plus 180-kDa cleaved form) were quantified using FLA-5000 (Fujifilm). Radioactivities in the absence of orthovanadate were subtracted from radioactivities in the presence of orthovanadate and presented as means ± SD after normalization to the level of ABCA3-GFP protein (total 220-kDa noncleaved form plus 180-kDa cleaved form). Statistical analysis was performed as described above.

Photoaffinity labeling of ABCA3-GFP and mutant proteins with 8-azido-[γ-^{32}P]ATP or 8-azido-[α-^{32}P]ADP. A 20,000-*g* membrane fraction was incubated with 40 μM 8-azido-[γ-^{32}P]ATP or 8-azido-[α-^{32}P]ADP, 2 mM ouabain, 0.1 mM EGTA, 3 mM $MgCl_2$, and 40 mM Tris·HCl (pH 7.5) in a total volume of 12 μl for 10 min at 0°C. After irradiation for 5 min (254 nm, 8.2 mW/cm^2) on ice, 400 μl of TEM buffer were added and supernatant containing unbound nucleotides was removed from the membrane pellet after centrifugation (20,000 *g*, 10 min, 2°C). The pellets were solubilized in RIPA buffer [50 mM Tris·HCl (pH 7.5), 150 mM NaCl, 1 mM EDTA, 1% Nonidet P-40, 0.1% SDS, and 0.5% sodium deoxycholate] containing protease inhibitor mixture for 30 min at 4°C. After centrifugation (20,000 *g*, 20 min, 2°C), proteins were immunoprecipitated from the supernatant with the anti-human ABCA3 antibody (38). Samples were electrophoresed on a 5% SDS-polyacrylamide gel and transferred to a PVDF membrane. The radioactivities of photoaffinity-labeled protein (total 220-kDa noncleaved form plus 180-kDa cleaved form) were quantified using FLA-5000. To confirm the expression level of ABCA3-GFP proteins, the membrane was further analyzed by immunoblotting using anti-GFP antibody. Data normalized to the level of ABCA3-GFP proteins (total 220-kDa noncleaved form plus 180-kDa cleaved form) are presented as means ± SD. Statistical analysis was performed as described above.

Homology modeling of nucleotide binding domain 1 of ABCA3. The secondary structures of nucleotide binding domains (NBDs) of ABCA3 and other ABC transporters were predicted using the PSIPRED program (19). Amino acids sequences were aligned using the ClustalW program (15) and manually corrected based on the predicted secondary structures. The amino acids residues 545–766 in NBD-1 of ABCA3 share 29.7%, 25.7%, and 23.4% sequence identities with *Escherichia coli* maltose transporter MalK, *Staphylococcus aureus* Sav1866, and *E. coli* hemolysin transporter HlyB, respectively (6, 9, 39). The structure of NBD-1 of ABCA3 was modeled based on the ATP-bound closed form of *E. coli* MalK (Protein Data Bank entry 1Q12; Ref. 6) using SWISS-MODEL (26). Amino acid substitution was performed on Swiss-PDB Viewer, considering the best rotamer conformation.

RESULTS

Subcellular localization and glycosylation of ABCA3-GFP and pILD mutant proteins. We previously found that GFP-tagged wild-type ABCA3 protein (ABCA3-GFP) expressed in cultured cells is localized mainly at the limiting membrane of LAMP3-positive vesicles, whereas type I mutant protein (e.g., L101P) in fatal surfactant deficiency remains localized in the endoplasmic reticulum, accompanied by impaired processing of oligosaccharide (17). The E292V, E690K, and T1114M mutations identified in pILD (4) are located at intracellular loop 1 (ICL-1), adjacent to the Walker B motif in NBD-1 and the 8th putative transmembrane segment (TM-8), respectively (Fig. 1*A*). When E292V, E690K, and T1114M mutant ABCA3-GFP proteins were transiently expressed in HEK-293 cells, most of the GFP fluorescence was located at intracellular vesicles, as with the wild-type protein (Fig. 1*B*). ABCA3 is expressed as 190- and 150-kDa forms, with the latter suggested to be produced by proteolytic cleavage at extracellular domain 1 (ECD1) within lysosomal vesicles (21, 36). In native lung tissue, the cleaved form is predominant, whereas both forms are detected when overexpressed in cultured cells. Immunoblot analysis of total membrane fraction from transiently transfected HEK-293 cells using anti-GFP antibody showed two bands at ~220 kDa (noncleaved form) and 180 kDa (cleaved form) in wild-type and three mutant ABCA3-GFP proteins (Fig. 1*C*). In E690K mutant protein, the amount of the 180-kDa cleaved form was increased compared with that of wild-type protein. PNGase F digestion of total membrane fraction showed that the 220-kDa forms of all three mutants are *N*-glycosylated, as is wild-type

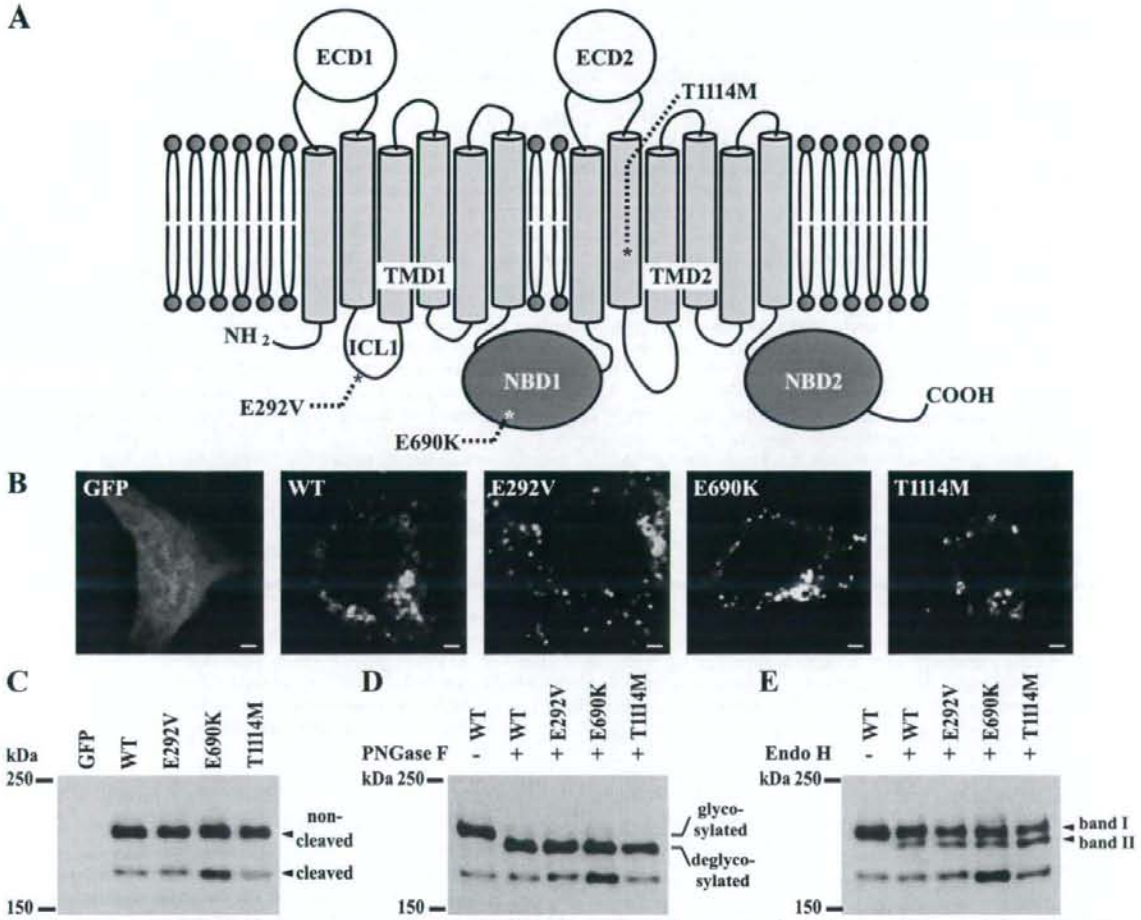

Fig. 1. Structural model of ATP-binding cassette transporter ABCA3 protein and intracellular localization and glycosylation of wild-type ABCA3-green fluorescent protein (GFP) and pediatric interstitial lung disease (pILD) mutant proteins. *A*: locations of pILD mutations characterized in this study are indicated. ABCA3 is constituted by 2 transmembrane domains (TMD), each of which contains 6 putative transmembrane segments (TM), 2 extracellular domains (ECD), and 2 nucleotide binding domains (NBD). There are 3 asparagine residues (Asp53, Asp124, and Asp140) with a consensus *N*-glycosylation motif (NXS/T) in ECD1 but not in ECD2. *B*: intracellular localization of GFP, wild-type ABCA3-GFP protein (WT), and its mutants (E292V, E690K, and T1114M) transiently expressed in human embryonic kidney HEK-293 cells were determined by confocal microscopy. Scale bar, 2 μm. *C*: total membrane fractions from HEK-293 cells transiently transfected with GFP, WT ABCA3-GFP, or mutants were subjected to SDS-PAGE, transferred to polyvinylidene difluoride (PVDF) membranes, and analyzed using anti-GFP monoclonal antibody. The positions of noncleaved (220 kDa) and cleaved (180 kDa) ABCA3-GFP proteins are indicated. *D*: total membrane fraction with (+) or without (−) treatment of peptide *N*-glycosidase F (PNGase F) was subjected to SDS-PAGE and analyzed by immunoblotting. ABCA3-GFP proteins modified with oligosaccharide (220 kDa) were deglycosylated by PNGase F, producing 210-kDa proteins. *E*: total membrane fraction with or without treatment of endoglycosidase H (Endo H) was subjected to SDS-PAGE and analyzed by immunoblotting. *Band I* shows Endo H-insensitive 220-kDa ABCA3-GFP proteins containing complex-type sugar chains, whereas *band II* shows Endo H-sensitive 210-kDa proteins modified with high-mannose-type sugar chains.

ABCA3-GFP protein (Fig. 1*D*). In the E292V, E690K, and T1114M mutant proteins, 50–60% of the 220-kDa protein remained as Endo H-insensitive complex-type protein (Fig. 1*E*), indicating that intracellular trafficking and processing of oligosaccharide of these mutant proteins are largely preserved and that these mutations are not type I mutations.

Lipid transport function of ABCA3-GFP and pILD mutant proteins. The lipid transport function of ABCA3 protein has been investigated using non-lung HEK-293 cells or lung adenocarcinoma A549 cells transfected with ABCA3 (7, 18). In this study, we established HEK-293 cells stably expressing pILD mutant ABCA3-GFP proteins that can be used to analyze both lipid transport function and nucleotide trapping of ABCA3 proteins. ABCA3 mediates uptake of choline-phospholipids into LAMP3-positive vesicles to convert lysosomal organelles into lamellar body-like organelles (7, 18). The lipid transport function of ABCA3 protein can therefore be evaluated by comparing endogenous content of choline-phospholipid-rich vesicles and the level of LAMP3, a marker of lysosomal organelles such as multivesicular bodies and lamellar bodies (34, 35). Expression of wild-type ABCA3-GFP in HEK-293 cells was found to increase the level of LAMP3, as well as the

choline-phospholipid level and low-density and choline-phospholipid-rich vesicle contents (Fig. 2, *A*, *B*, and *D*), as we previously found in A549 cells (18). Immunoblot analysis using anti-GFP antibody revealed that three mutant ABCA3-GFP proteins were expressed at a level similar to that in wild-type protein (Fig. 2*A*). The level of LAMP3 in E292V transfectant was comparable to that in wild-type transfectant, whereas those in E690K and T1114M transfectants were lower than in wild-type transfectant (Fig. 2*A* and Supplemental Fig. 1*A*). (Supplemental data for this article is available online at the *American Journal of Physiology-Lung Cellular and Molecular Physiology* website.) The smeared appearance of the immunoblot signal reflects high glycosylation states of LAMP3 protein (16). On the other hand, the levels of GRP78, a marker of endoplasmic reticulum, were similar in the five cell lines. These results indicate that expression of pILD mutant ABCA3-GFP proteins affects lysosomal organelles in differing degrees.

To investigate the effect of ABCA3 expression on the endogenous lipid level, we analyzed the contents of choline-phospholipids and total cholesterol in these cell lines. The levels of choline-phospholipids were significantly increased 1.38- and 1.13-fold in wild-type and E292V transfectants, respectively, compared with the level in HEK-293 cells, whereas levels in E690K and T1114M transfectants were similar to that in HEK-293 cells (Fig. 2*B*). On the other hand, the levels of total cholesterol were similar in the five cell lines (Fig. 2*C*).

We then investigated sucrose gradient fractionation to identify low-density and choline-phospholipid-rich vesicle formation in mutant transfectants. In this gradient system, choline-phospholipid-rich vesicles generated by ABCA3-mediated lipid transport migrate to the lower fractions in a manner similar to lamellar bodies from native lung tissue (18). In wild-type transfectant, endogenous choline-phospholipid content in the lower fractions (*fractions 2–4*) was higher than in HEK-293 cells (Fig. 2*D*). In addition, in wild-type transfectant, LAMP3 was detected mainly in *fractions 2–4* and *10*, whereas LAMP3 was detected mainly in *fraction 10* and partly in *fractions 4–6* in HEK-293 cells (Supplemental Fig. 1*B*). Thus the increased choline-phospholipid content in the lower fractions and the shift of LAMP3 distribution into lower fractions reflect ABCA3-mediated uptake of choline-phospholipids into LAMP3-positive vesicles to convert lysosomal organelles into lower density and lipid-rich vesicles (7, 18). In E292V transfectant, choline-phospholipid content in *fractions 2–4* was higher than that in HEK-293 cells and lower than that in wild-type transfectant. In E690K transfectant, the distribution of choline-phospholipid content was similar to that in HEK-293 cells. In T1114M transfectant, choline-phospholipid content in *fractions 2–4* was somewhat higher than that in HEK-293 cells, but the difference was not statistically significant ($n = 4$, Supplemental Fig. 1*C*). Considered together, these results suggest that although the lipid transport function of the E292V mutant protein is moderate, those of the E690K and T1114M mutant proteins are severely impaired.

Abnormalities of ATP binding and/or hydrolysis in pILD mutant proteins. To clarify the mechanism of impaired lipid transport in the pILD mutant proteins, we compared ATP

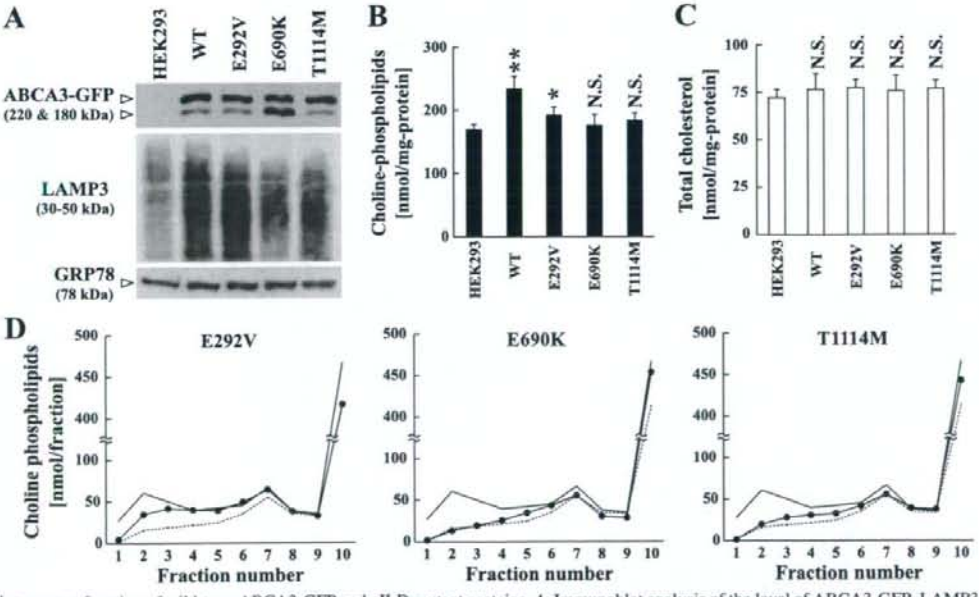

Fig. 2. Lipids transport function of wild-type ABCA3-GFP and pILD mutant proteins. *A*: Immunoblot analysis of the level of ABCA3-GFP, LAMP3, and GRP78 in HEK-293 cells stably expressing WT ABCA3-GFP, E292V, E690K, T1114M, or untransfected HEK-293 cells. *B* and *C*: the contents of endogenous choline-phospholipids (*B*) and total cholesterol (*C*) in postnuclear supernatant (PNS) of each cell type. Data are means ± SD ($n = 6–9$). *$P < 0.05$; **$P < 0.01$ vs. HEK-293 cells. N.S., not significant. *D*: sucrose gradient fractionation of intracellular compartments from each cell type. PNS (4 mg of protein) was fractionated in a sucrose gradient. *Fractions 1* and *10* are the lowest and highest density fractions, respectively. The contents of endogenous choline-phospholipids are shown. For comparison, the lipid content of HEK-293 cells stably expressing wild-type ABCA3 (solid line) and untransfected HEK-293 cells (broken line) are shown. Experiments were performed 4 times, and representative data are shown.

hydrolysis of these mutants by using a vanadate-induced nucleotide trapping technique (28, 32). ABCA3 protein efficiently traps Mg-ADP in the presence of orthovanadate, an analog of phosphate, and forms a stable inhibitory intermediate during the ATP hydrolysis cycle (17, 21). This intermediate can be specifically photoaffinity labeled in the membrane after ATP hydrolysis when 8-azido-[α-^{32}P]ATP is used as an ATP analog, allowing assessment of ATP hydrolysis with production of a stable intermediate based on the intensity of photoaffinity labeling.

As previously reported (17), among 20,000-*g* membrane fractions of cells expressing wild-type ABCA3-GFP, 220-kDa (noncleaved form) and 180-kDa (cleaved form) proteins were slightly photoaffinity labeled with 8-azido-[α-^{32}P]ATP in the absence of orthovanadate (Fig. 3*A*, *lane 3*), and photoaffinity labeling was further induced in the presence of orthovanadate (Fig. 3*A*, *lane 4*). In vanadate-induced nucleotide trapping by the E292V and T1114M mutant proteins, ATP hydrolysis with production of a photoaffinity-labeled intermediate was decreased to 40 and 52% of that of wild-type protein, respectively (Fig. 3*A*, *lanes 5*, *6*, *9*, and *10*, and *B*). On the other hand, in the E690K mutant protein, it was increased to 200% of that of wild-type protein (Fig. 3*A*, *lanes 7* and *8*, and *B*).

To investigate the altered ATP hydrolysis with production of a photoaffinity-labeled intermediate in the mutant proteins, we examined ATP binding of ABCA3-GFP proteins by photoaffinity labeling with 8-azido-[γ-^{32}P]ATP at 0°C. In this nonhydrolytic condition, ABCA3-GFP proteins are labeled only with nucleotides before hydrolysis, allowing determination of ATP binding based on the intensity of photoaffinity labeling. Among the 20,000-*g* membrane fractions of cells expressing wild-type ABCA3-GFP, 220- and 180-kDa proteins were photoaffinity labeled with 8-azido-[γ-^{32}P]ATP, whereas membrane fractions of untransfected cells were not photoaffinity labeled (Fig. 3*C*). ATP binding of the E292V and T1114M mutant proteins determined by photoaffinity labeling with 8-azido-[γ-^{32}P]ATP was similar to that of wild-type ABCA3-GFP protein (Fig. 3, *C* and *D*). However, in E690K mutant protein, photoaffinity labeling of the 220-kDa protein was similar to that of wild type protein regardless of decreased noncleaved form protein, and photoaffinity labeling of the 180-kDa protein was dramatically enhanced even when the increased levels of the cleaved form of the protein were taken into consideration. When normalized to the level of ABCA3-GFP proteins (total 220-kDa noncleaved form plus 180-kDa cleaved form), photoaffinity labeling of the E690K mutant protein was increased to 250% of that of wild-type protein. These results show that the catalytic cycles of these mutant proteins differ from that of wild-type protein and that these mutations in pILD are type II mutations.

Mutational analysis of Glu292 in ICL-1 and Thr1114 in putative TM-8. To investigate the mechanism of loss of ATP hydrolysis with production of a photoaffinity-labeled intermediate in E292V and T1114M mutant proteins, we performed mutational analyses of Glu292 residue in ICL-1 and Thr1114 in putative TM-8. The Glu or Asp residue in ICL-1 is conserved in members of the ABCA subfamily (Fig. 4*A*), suggesting the importance of negatively charged amino acids in ICL-1 for ATP hydrolysis. To clarify this, we substituted Glu292 with Asp and Lys, which are negatively and positively charged, respectively. In vanadate-induced nucleotide trapping by E292D mutant protein, production of a photoaffinity-labeled

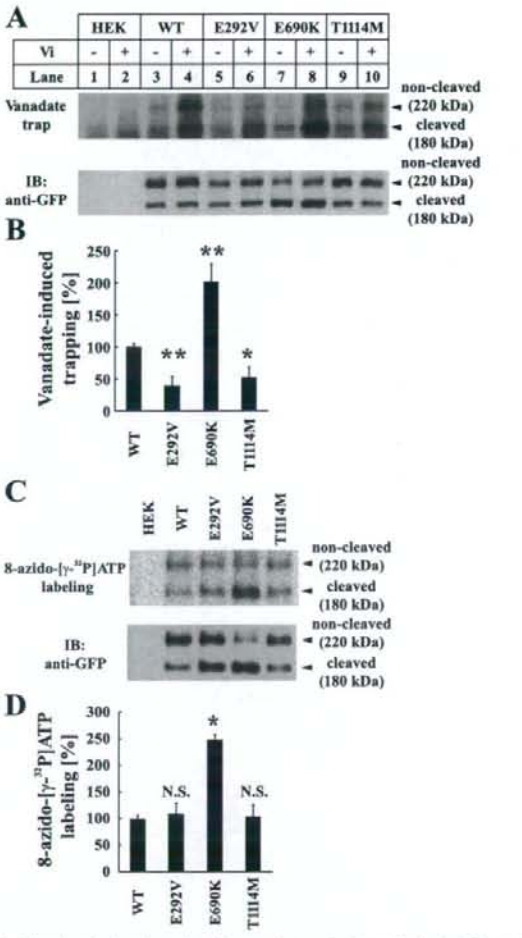

Fig. 3. Vanadate-induced nucleotide trapping and photoaffinity labeling of ABCA3-GFP and pILD mutant proteins using 8-azido-[^{32}P]ATP. *A*: 20,000-*g* membrane fraction prepared from HEK-293 cells stably expressing the WT ABCA3-GFP (*lanes 3* and *4*), E292V (*lanes 5* and *6*), E690K (*lanes 7* and *8*), T1114M (*lanes 9* and *10*), or untransfected HEK-293 cells (*lanes 1* and *2*) was incubated with 10 μM 8-azido-[α-^{32}P]ATP in the absence (−) or presence (+) of 0.4 mM orthovanadate (Vi) and 3 mM $MgCl_2$ for 10 min at 37°C. Protein was photoaffinity labeled with UV irradiation after removal of unbound ATP, electrophoresed on SDS-PAGE, and transferred to a PVDF membrane. Membrane was analyzed by autoradiography (*top*) and immunoblotting (IB) using anti-GFP antibody (*bottom*). *B*: radioactivity of photoaffinity-labeled protein (total 220-kDa noncleaved form plus 180-kDa cleaved form) was quantified by FLA-5000. Radioactivity in the absence of orthovanadate was subtracted from that in the presence of orthovanadate and is expressed after normalization to the level of ABCA3-GFP protein (total 220-kDa noncleaved form plus 180-kDa cleaved form). Data are means ± SD (n = 4). *P < 0.05; **P < 0.01 vs. WT. *C*: 20,000-*g* membrane fraction prepared from HEK-293 cells stably expressing the WT ABCA3-GFP, E292V, E690K, T1114M, or untransfected HEK-293 cells was incubated with 40 μM 8-azido-[γ-^{32}P] and 3 mM $MgCl_2$ for 10 min at 0°C. Protein was photoaffinity labeled with UV irradiation, immunoprecipitated with anti-human ABCA3 antibody, electrophoresed on SDS-PAGE, and transferred to a PVDF membrane. Membrane was analyzed by FLA-5000 (*top*) and IB using anti-GFP antibody (*bottom*). *D*: radioactivity of photoaffinity-labeled protein (total 220-kDa noncleaved form plus 180-kDa cleaved form) was quantified by FLA-5000 and is expressed after normalization to the level of ABCA3-GFP protein (total 220-kDa noncleaved form plus 180-kDa cleaved form). Data are means ± SD (n = 3). *P < 0.01 vs. WT.